Proceedings World Geothermal Congress 2015
Melbourne, Australia, 19-25 April 2015

Experimental Assessment of Cement Integrity under Geopressured Geothermal Reservoir Conditions

Mileva Radonjic and Kolawole S. Bello

Craft and Hawkins Department of Petroleum Engineering, 2131 Patrick F. Taylor Hall, Louisiana State University, Baton Rouge, LA 70802

mileva@lsu.edu

Keywords: Geothermal Wellbore Cement, Strength Retrogression, Liquid Pressure-Pulse Decay Permeameter, Zonal isolation

ABSTRACT

Geopressured reservoirs in the northern Gulf of Mexico basin along the coast of Louisiana have been identified to be potential source of geothermal energy. These reservoirs are made of unconsolidated sandstone capped by shale layers and possess temperatures as high as 140 ^{0}C. Salinity values reaching a high of 100 g/L are associated with these reservoirs due to the dissolution of surrounding salt domes. Currently, novel wellbore system with downhole heat exchanger is being developed for in-situ heat harvesting that would result in zero-mass withdrawal. The techniques for heat extraction from geopressured geothermal reservoirs involve production of hot water and injection of cold water into the wellbore, which expose downhole materials to harsh temperature variations. Heating and cooling make the cement expand and contract as a result of thermal expansion. This volumetric change can initiate cement fractures, leading to failure of annular cement sheath resulting in well integrity issues and subsequently lead to lack of zonal isolation and compromised wellbore mechanical properties.

This study measures the effect of cyclic thermal loading on cement slurry designs exposed to brines representative of the local geofluids. Grain volume porosimeter and Liquid Pressure-pulse Decay Permeameter were used to quantify the presence of thermal fractures as they are capable of measuring porosity and brine permeability of cement under reservoir conditions. Scanning Electron Microscopy micrographs with Energy Dispersive Spectroscopy capabilities, and Thermogravimetric analysis were used to study the microstructural and compositional changes in the cement slurry designs. Five cement designs with a range of chemical additives/fibers were subjected to 100 thermal cycles from 90 to 40^{0}C at 100% relative humidity in brine. The experimental results indicate leaching of $Ca(OH)_2$ will occur from the cement irrespective of cement composition which causes the porosity and permeability of the cement sheath to increase. Due to the thermal cycling, the strength of the cement sheath decreases as a result of mineralogical alteration that is accompanied with lower compressive strength. The study also shows that glass fiber and steel fiber can be added to the design to reduce the permeability and increase the strength of the cement sheath under thermal cycle loading conditions although they would not prevent it from completely degrading as the well ages, but will increase the service life of the wellbore under given conditions.

1. INTRODUCTION

Geothermal systems serve as ample sources of sustainable carbon-free energy used in the generation of electricity, space heating and air conditioning. Geopressured aquifers, a type of geothermal systems, are undercompacted brine saturated porous and permeable formations that have anomalously high pore pressures and moderate temperatures. In the Gulf of Mexico, geopressured reservoirs form as a result of rapid sediment loading from river-borne systems and their deltas. The penetration of sands into underlying muds resulted in isolation of large sand members from the overlying strata. The weight of the sediment layer on the trapped fluids results in elevated pore pressures. These isolated units of sands and muds contain pore pressure of 15.269 kPa/m (0.675psi/ft.), or higher comparing to an average of 0.475 psi/ft commonly used in these locations (Griggs, 2004). In addition, expulsion of water into sands from underlying shale as montmorillite converts to illite contributes to the elevated pressure (Dorfman, 1982). Temperatures in geopressured reservoir typically range from 90^{0}C to 200+^{0}C with salinities as high as 100 g/L (Hanor and Mercer, 2010). Camerina Sand A, a geopressured geothermal reservoir in Vermilion Parish, Louisiana (McCoy et al., 1980) is used as a case study in this research and brine composition used in the lab was a replica from this field. The main concern with producing these geopressured reservoirs pertains to the environmental changes brought about by the removal of vast amounts of high-pressure and the subsequent decrease in reservoir pressures, cooling and migration of subsurface water near the wellbore and.potential mineral dissolution/precipitation in the reservoir. This can result in surface subsidence or worse induce an earthquake (Herrin, 1975). Novel wellbore system with downhole heat exchanger is been investigated for in-situ heat harvesting resulting in zero-mass withdrawal that would reduce the mentioned risk (Feng et al., 2010).

Drilling and completing high temperature wellbores is always a challenge due to the durability of materials and lack of compatibility of wellbore cements with physical and chemical environments associated with geothermal conditions. Portland cement is the main component used in wellbore cement slurries. It is used for primary cementing, wellbore remediation and plug and abandonment of wells. Hardened cement is formed by mixing unhydrated cement clinker with water. Upon complete hydration, the two main hydration products are: calcium silicate hydrate and calcium hydroxide. The concentration of the mineral phases in the unhydrated cement as well as the hydration temperature determines the rate of hydration, the strength and the permeability of hydrated product. Calcium silicate hydrate is the main binding phase and thus influences strength in hydrated cement (Taylor, 1997). Cement is a porous material with highly alkaline (pH~13) pore solution (pore water), depending on the water to cement ratio. The alkalinity maintains the calcium hydroxide in the cement matrix. The higher the degree of hydration, the lower the porosity and permeability as more calcium silicate hydrate is formed. The cement hydration is highly sensitive to water to cement ratio (w/c) and to temperature, to a lesser degree pressure conditions.

The most important purpose of cementing a wellbore is zonal isolation. Failures in cement sheaths can lead to the contamination of fresh water aquifer, migration of reservoir fluids from high pressure sands to low pressure sands and sustained casing pressure as a result of fluid migration from the reservoir to the surface. Production and injection of geofluids in proposed geothermal well will result in thermal loading of the cement possibly causing fractures within the cement sheath and de-bonding at cement/casing and cement/formation interfaces. This changes the structure of the hydrated cement leading to increased porosity, permeability and lowered compressive strength (Taylor, 1997). The real problem lies in the great increase of permeability as it makes the cement susceptible to corrosive formation fluids (Sugama, 2006). Experimental studies by Yalkinkaya et al. (2011) shows that exposure of cement fracture to CO_2 rich brine will increase the porosity and widen the fracture. The research also suggests that in time when exposed to low pH fluids, cement/formation interfaces (Berea sandstone) will become more permeable and have lower shear bond strength (Agbasimalo and Radonjic, 2014; and Oyibo and Radonjic, 2014).

2. EXPERIMENTAL MATERIALS AND PROCEDURE

To study the behavior of cement in proposed zero-mass withdrawal wellbore (Feng et al, 2011), a batch experiment was conducted using 4 different class H cement slurry designs, tabulated below (Table 1.) Four 13.1 pounds per gallon (ppg) (1.31 g/cc) cement slurry designs with cement additives to accommodate for the severe environmental conditions were investigated and compared with 13.1 ppg neat cement slurry (control sample with no additives). All four cement slurry designs contain class H cement and silica flour. Fine calcined clay, silica sand, steel fiber and glass were added to the first, second, third and fourth sample respectively (Table 1). The calcined clay has a grain size ranging from 45 microns to 75 microns. The calcined clay and steel fiber have a size range of 5 microns and 400 microns respectively. The glass fiber has the biggest grain size of the additives with a range of 3-5mm. The chemical additives were added to Portland cement slurry to counteract and curb strength retrogression, by changing cement hydration products into chemically more stable phases, with favorable Ca to Si ratio. The selected additives were also chosen because of their potential to prevent thermal micro fracturing of cement sheath. Cement core samples were made according to the American Petroleum Institute (API) recommended practice API-10B, (American Petroleum Institute, 1977).

Table 1: Mix proportions of cement slurries by mass. Slurries were mixed using water to solid ratio of 0.87 to achieve slurry density of 13.1 ppg. For cement with additive, there was 35% weight replacement of cement with silica flour.

Design	Class H Cement	Bentonite	Silica Flour	Steel Fiber	Silica Sand	Calcined Clay	Glass Fiber	Water
Neat Cement (control sample)	1	0.02	-	-	-	-	-	0.87
Steel Fiber Cement	1	0.02	0.35	0.02	-	-	-	1.17
Silica Sand Cement	1	0.02	0.35	-	0.02	-	-	1.17
Calcined Clay Cement	1	0.02	0.35	-	-	0.02	-	1.17
Glass Fiber Cement	1	0.02	0.35	-	-	-	0.02	1.17

The cement slurry was prepared by mixing Class H cement and distilled water at a water to solid ratio of 0.87. The mixing was done with a four liter, 3.75 horsepower Waring® blender. Bentonite and water was mixed first at 16,000 revolutions per minute (RPM). After 5 minute, the rest of the material was added to the mixture in the blender and mixed at 20,000 RPM for the next 35 seconds. The cement slurry was poured into 3 in. X 1 in. cylindrical brass molds. The wait on cement period was 24 hours after which the cement cores were de-molded and used in the experiments.

Hydrated cement cores were subjected to cycles of differential temperature of 50^0C with 100% relative humidity (RH) in experimental brine (Table 2) using temperature cycling/relative humidity (environmental) chamber. Each cycle took 12 hours with the temperature ramped from 40^0C to 90^0C and back to 40^0C. The environmental chamber is an ESPEC EGNL12-4CAL model with a lower and upper temperature limit of -40^0C and 180^0C respectively. The experiment was limited by the boiling point of water, and that was why it was conducted at 90^0C rather than over 100^0C to simulate field conditions of 140C.

Table 2: Brine Composition for Experiments. The brine was designed to simulate the fluid composition of Camerina sand.

Salts	Amount mixed with 1L of distilled water
Sodium Chloride (NaCl)	32.19 g
Potassium Chloride (KCl)	0.454 g
Magnesium Chloride ($MgCl_2$)	0.991 g

The porosity, density, permeability and compressive strengths of the samples were taken before and after 100 cycles. The porosity and density was measured using a Ultragrain Grain Volume Porosimeter, UGV-200 from Core Laboraties. The UGV-200 utilizes Boyles Law helium gas expansion porosimetry. 10 cc of helium gas at a certain pressure is expanded into the cement cores. The final pressure occupied by the gas is then used to determine the grain volume of the cement cores. The grain volume with the bulk volume of the core is then used to determine the porosity of the cement cores. The grain volume and the weight of the cores are also used to determine the density of the hydrated cement cores. The bulk volumes of the cores were calculated from the core dimensions taken with a caliper while the weight of the cores are measured using a mass balance.

Laboratory measurement of low permeability media such as cement to water is usually a technical challenge. A liquid pressure-pulse decay permeameter model CFS-200 was used to determine the permeability of the cement cores as it employs a transient

technique to measure cement permeability to water. Cores are placed in a pressure vessel that allows hydrostatic confining pressures as high as 680 bar (10000 psi), maximum back pressure of 400 bar (6000 psi) and resist temperatures to ~ 150 ^{0}C. The permeability is a function of pressure decay through the core over time using semilog analysis (Jones, 1997; Chen and Stagg, 1984). The permeability was reported in nanoDarcy (nD) (equivalent to 10^{-21} m^2).

Compared to conventional (steady state) methods, the liquid pressure-pulse decay permeameter cuts down the long time required to stabilize water fluxes from days or weeks to hours that is typical for low permeability materials such as Portland Cement based composites. This is very critical as cement permeability could change due to leaching or hydration during the time required in steady state methods (Scherer et al., 2006; Boulin et al., 2012).

A Model 4207D Compressive Strength Testers would be used to measure the unconfined maximum compressive strength of hydrated cement cores after 100 thermal cycles according to the API RP 10A (American Petroleum Institute, 1977). This was done in order to quantify the effect of thermal cycle loading on the strength of the cement.

Thermogravimetric Analysis (TGA) was used to determine the weight change of calcium hydroxide within each cement sample design. Small samples were cut from the cores, dipped in acetone to remove any surface water present and grounded using an agate mortar and pestle. TA Instruments SDT Q600 Simultaneous DSC/TGA was used from ambient to 1500°C (2732°F). The following parameters were used in the analysis: purge gas of nitrogen at a flow rate of 0.0035 ft^3/min (100 ml/min); alumina pans; equilibration at 40°C (104°F) for 10 minutes; heating rate of 5°C/min (41°F/min) from 40°C (104°F) to 200°C (392°F) , followed by a heating rate of 10°C/min (50°F/min) up to 1000°C (1832°F).

3. RESULTS

3.1 Cement Porosity

Porosity was determined on three cores from each sample design using a Helium Boyle's Law Porosimeter. The cores were trimmed down to approximately 5.08 cm. (2 in.) length and 2.54 cm. (1 in.) in diameter. Table 3 summarizes the porosity of the four designs after 100 cycles. Steel cement design exhibit the least porosity with an average of 53.64%. The highest porosity average was 57.61% measured in glass fiber cement cores. A cement core containing glass fiber had the highest porosity at 58.34% while a cement core containing steel fiber had the least porosity of 51.03%. It should be noted that the density of the steel cement core with the least porosity was smaller compared to the rest of the cores. The porosities of the all the cores were very similar with a range of 7.31% and a smaller range of 2.98% if the 51.03% porosity measured in one the steel fiber samples was not considered.

Table 3: Average density and average porosity of cement sample designs. Neat cement design had the highest porosity while steel fiber cement design possessed the least porosity.

Design	Average Density (g/cc)	Average Porosity (%)
Neat Cement	2.343±0.015	57.41±0.608
Steel Fiber Cement	2.363±0.072	54.36±2.895
Silica Sand Cement	2.382±0.018	56.56±0.421
Calcined Clay Cement	2.400±0.034	55.63±0.238
Glass Fiber Cement	2.397±0.041	56.97±1.328

3.2 Cement Permeability

Permeability was carried out on wet cement cores after 100 thermal loading cycles using a liquid pulse pressure decay permeameter. Permeability in all cement designs were close in the 10^{-6} - 10^{-7} D range. Glass fiber cements had the least permeability with an average of $9.241x10^{-08}$ D. Silica sand cements had the highest average permeability at $3.966 x10^{-07}$ D. Table 4 shows the average permeability value of each cement design.

Table 4: Average permeability of the cement designs after 100 thermal loading cycles. Silica sand cement design exhibit the highest permeability while glass fiber cement design has the least permeability.

Design	Average Permeability (D)	Average Permeability (m^2)
Neat Cement	$3.052x10^{-07}$±$2.885x10^{-08}$	$3.012x10^{-19}$±$2.847x10^{-20}$
Steel Fiber Cement	$2.577x10^{-07}$±$2.351x10^{-08}$	$2.543x10^{-19}$±$2.320x10^{-20}$
Silica Sand Cement	$3.966x10^{-07}$±$4.028x10^{-08}$	$3.914x10^{-19}$±$3.975x10^{-20}$
Calcined Clay Cement	$2.897x10^{-07}$±$6.000x10^{-08}$	$2.859x10^{-19}$±$5.922x10^{-20}$
Glass Fiber Cement	$9.241x10^{-08}$±$6.527x10^{-08}$	$9.120x10^{-20}$±$6.442x10^{-20}$

3. 3 Cement Compressive Strength

The Unconfined Compressive Strength Tester measures the maximum force required to produce failure under compression in the cement core. The maximum force is divided by the cross sectional area of the cement core to derive the compressive strength. Two cores from each design were tested for strength. A summary of the results is presented in Table 5. This data is of a semi-quantiative nature, the accurate measurement that replicates field conditions would have to be confined compressive test in a tri-axial load cell.

Table 5: Average compressive strength of the cement designs based on 3 measurements. Cement designs with steel fibers exhibit the most compressive strength while cement designs with glass fibers have the least compressive strength.

Design	Average Compressive Strength (MPa)
Neat Cement	2.822±1.144
Steel Fiber Cement	3.034±0.539
Silica Sand Cement	2.879±1.333
Calcined Clay Cement	2.794±1.081
Glass Fiber Cement	1.989±0.919

3.4 Scanning Electron Microscope (SEM) and Energy Dispersive Analysis (EDS)

SEM was carried out to observe the microstructures of core of each design after 100 thermal cycles. SEM micrographs showed that the mineral composition of the designs were very similar. In the neat cement (Figure 1A), C-S-H, $Ca(OH)_2$ and unhydrated cement clinker dominated the microstructure. The C-S-H observed in the neat cement clinker was very coarse, large and fibrous. Figure 1B shows SEM and EDS analysis performed on steel fiber cement sample. The figure shows that the sample is dominated by quartz and C-S-H. The structure of this C-S-H is different from that observed in the neat cement sample, as they are less fibrous and porous. The steel fiber can be observed in low magnification micrographs because of their grain size. They are well dispersed through the cement matrix and appeared to have kept their shapes and sizes

The composition of the silica sand cement was similar to the steel fiber cement (Figure 1C). Large bulky quartz as well C-S-H were observed and confirmed in the SEM and EDS respectively. A closer look at the C-S-H shows that they have internal porosity. Na and Cl rich grains were present in the C-S-H structure (Figure 1F). Figure 1D are SEM micrographs of the calcined clay cement. Seedlets were observed on the surface of the quartz in micrographs.

Figure 1E contain SEM micrographs of glass fiber cement sample. The C-S-H in this sample was very fibrous compared to the rest of the cement design. In addition, large blob of material that appear to be glassy in nature were observed in the SEM micrographs. High amount of chlorine (Cl) was observed in EDS analysis of glass fiber, silica sand, steel fiber cement, and calcined clay cements especially in the pores.

3.5 Chemical Monitoring During and Post Thermal Cycle Loading

The pH and temperature of a control sample brine placed at ambient condition was taken after 45 days. The pH was measured to be 8.92 at 22.3^0C. Higher pH was measured in the experimental brines during the thermal cycle experiment. Table 6 shows the pH at respective temperature of the brines after 90 cycles of thermal loading.

Table 6: pH measurement of control brine after 45 days at ambient conditions and brine samples containing all the different samples after 90 thermal loading cycles. Higher pH measured in the brine containing cement samples suggests dissolution/leaching of cement matrix during thermal loading experiment.

Cement Design in Brine	Brine pH	Brine Temperature (^{0}C)
Control Brine	8.92	22.3
Neat Cement	11.27	61.3
Steel Fiber Cement	11.54	41.6
Silica Sand Cement	11.36	43.3
Calcined Clay Cement	11.42	45.8
Glass Fiber Cement	11.25	45.9

Figure 2 presents a plot of the analysis of the brine for common ions present in cement after 120 thermal cycles. Inductively Couples Plasma (ICP) mass spectrometry was used to detect the concentration of Al^{3+}, Ca^{2+}, Fe^{3+}, Mg^{2+} and Si^{4+}. There was an increase in the ions for all brines compared to the original brine except for Mg^{2+} which decreased. The most notable change was observed in the concentration of Ca^{2+} with almost three order of magnitude increase. Brines in contact with cement cores containing steel fiber and glass fiber cements had the highest concentration of Ca^{2+} with 1200 mg/L and 1202 mg/L respectively. Of significant importance is also the concentration of Si^{4+} observed. Brine with glass fiber cement Si^{4+} concentration of 18 mg/L which is the highest amongst the entire sample.

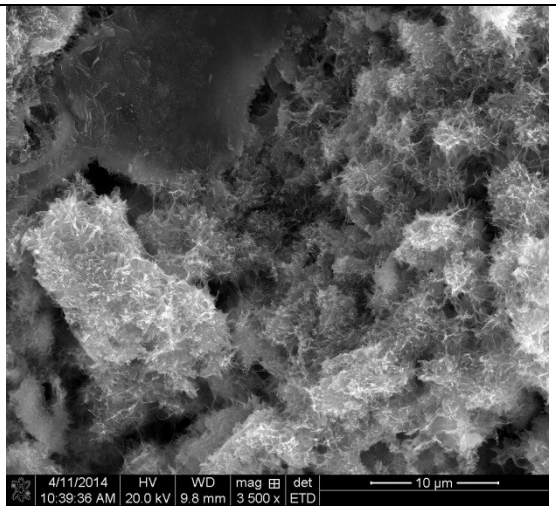

A. SEM image of cement sheath with no additive after 100 thermal loading cycles.

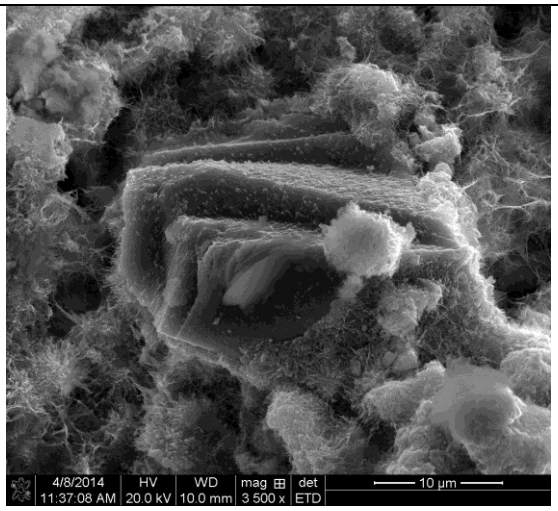

B. SEM image of cement sheath with silica flour and steel fiber after 100 thermal loading cycles.

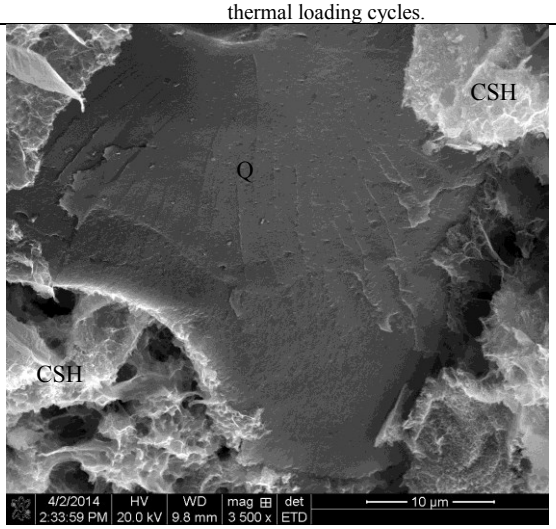

C. SEM image of cement hardened with silica flour and silica sand. Q stands for quartz while CSH is used to represent calcium silicate hydrate gel.

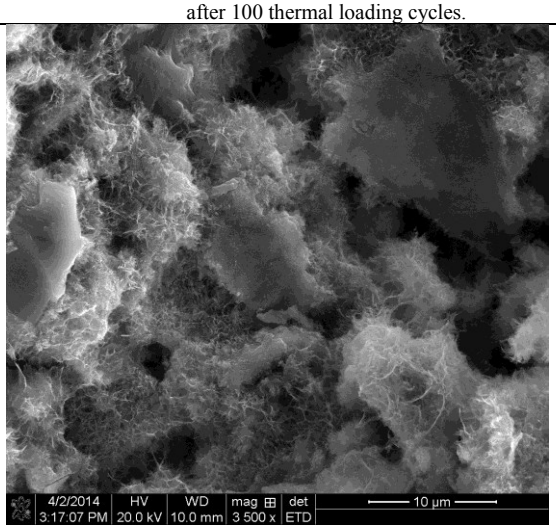

D. SEM image of cement sheath with silica flour and calcined clay after 100 thermal loading cycles.

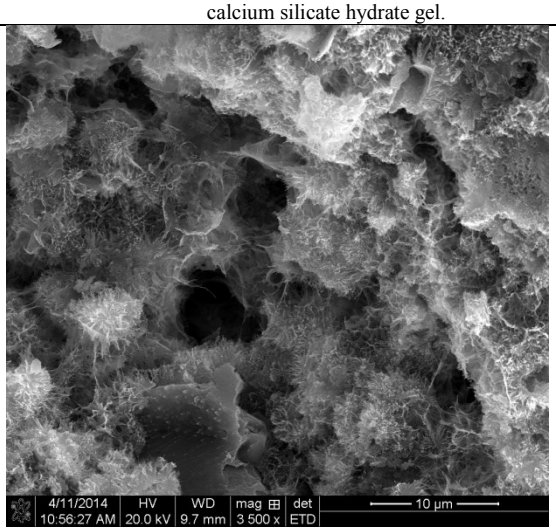

E. SEM image of hardened cement slurry after 100 thermal loading cycles

	Figure 6C Q Composition		Figure 6C CSH Composition	
Element	Weight %	Atomic %	Weight %	Atomic %
C	-	-	2.27	6.10
O	44.81	59.96	24.71	49.92
Al	0.11	0.08	-	-
Si	50.00	38.11	6.01	6.91
Cl	0.42	0.25	4.75	4.33
Ca	2.58	1.38	32.44	26.16
Fe	-	-	3.98	2.30

F. EDS analysis of Figure 6C showing the presence of quartz mineral (Q) and calcium silicate hydrate gel (CSH)

Figure 1: Scanning Electron Microscope (SEM) images of samples from cement design. While the mineral composition is similar in all the cement designs, the microstrure observed is different influencing the poro-mechanical properties. Figure 1F is an example of spatial composition used in confirming minerals observed in SEM images.

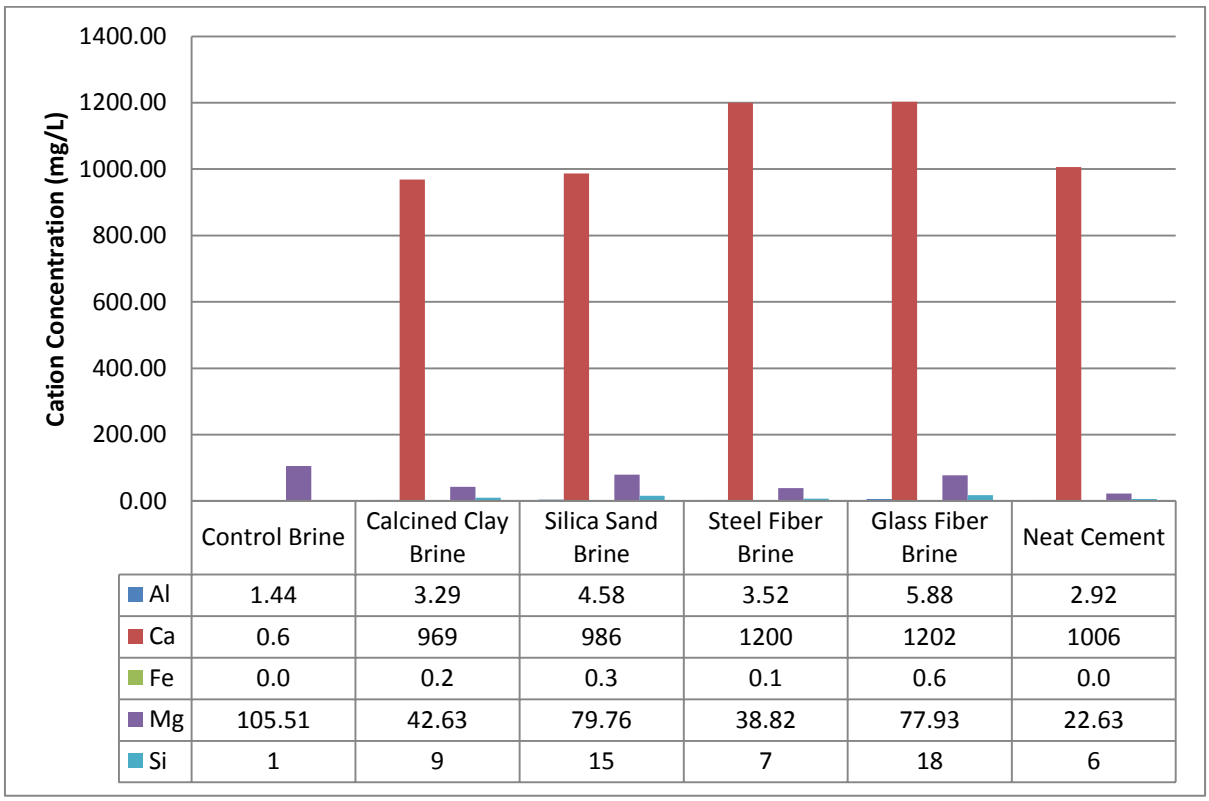

	Control Brine	Calcined Clay Brine	Silica Sand Brine	Steel Fiber Brine	Glass Fiber Brine	Neat Cement
Al	1.44	3.29	4.58	3.52	5.88	2.92
Ca	0.6	969	986	1200	1202	1006
Fe	0.0	0.2	0.3	0.1	0.6	0.0
Mg	105.51	42.63	79.76	38.82	77.93	22.63
Si	1	9	15	7	18	6

Figure 2: Inductively Coupled Plasma cation identification in brine containing different cement design after 100 cycles of thermal loading. Increase in Ca^{2+} and Si^{4+} in all the brines compared to the original brine indicate dissolution of main minerals in hydrated cement.

3.5 Thermogravimetric Analysis (TGA) of Cement Designs Post Experiment

TGA was run on the cement samples before and after 100 thermal loading cycles to quantify mineralogical changes in the cement composition as a result of thermal cycle loading. Two analyses were run on each cement design using sample from outer region of the core, which was in direct contact with the brine, and the sample from the inner region of the core, with no/or limited contact with brine. Neat, steel fiber, calcined clay and silica sand cements cores had more calcium hydroxide on the inside than on the surface which is in contact with the brine. Silica sand cement core had the opposite result. There was more calcium hydroxide on the surface than inside the core. Each graph represents individual design. Full lines represent data obtained on samples from the inner region of the core and dotted lines show data obtained from the outer region of each core.

Figure 3 shows comparison of the TGA from the outside and inside of the neat cement core after 100 thermal cycles. The peak at 421.25^0C is for $Ca(OH)_2$. From the outside of the core, weight loss of 2.664% at the calcium hydroxide peak indicates approximately 11% $Ca(OH)_2$ exist on the outside of the neat cement. On the inside of the neat cement core, weight loss of 3.233% was measured at the 421.25^0C peak which indicates approximately 13% $Ca(OH)_2$ exist on the inside of the neat cement. This result means more $Ca(OH)_2$ exist on the inside of the neat cement core.

Steel cement samples showed similar results to that of neat cement (Figure 4). TGA showed more $Ca(OH)_2$ exist on the inside than outside of the steel cement core. Weight loss of 1.698% was observed at the $Ca(OH)_2$ peak corresponding to the presence of approximately 7% of $Ca(OH)_2$ on the inside of the steel fiber. There was no significant weight loss on the outside of the core.

Figure 5 compares the chemical changes along the surface of the silica sand cement cores and the inside of the silica sand cement cores after 100 thermal cycle loading. The 1.347% weight loss at the 420^0C indicates that there is approximately 5% $Ca(OH)_2$ on the surface. This is greater than the amount of $Ca(OH)_2$ observed on the inside of the silica sand cement. A weight loss of 0.7254% was observed in similar temperature region, meaning only 3% $Ca(OH)_2$ remains on the inside of the silica sand cement.

TGA on samples from the inside and outside of a calcined clay core indicate higher amount of $Ca(OH)_2$ was removed from the outside of the calcined clay core than on the inside. A weight loss of 1.825% was measured on the sample from the surface of the calcined clay compared to 1.106% on sample from the inside of the calcined clay core (Figure 6). This corresponds to almost a 3 % change in the amount of $Ca(OH)_2$ present across the core.

Figure 7 depicts the result of TGA on the glass fiber cement core. Higher amount of $Ca(OH)_2$ was measured on the inside of the core than on the surface on the core. At 419^0C which is the $Ca(OH)_2$ peak, 1.934% was the weight loss measured on sample from the surface of the glass fiber core while a weight loss of 0.6903% was measured on the sample from the inside of the glass fiber core. This means that approximately 8% and 3% of the original $Ca(OH)_2$ present remained from the inside and outside of the glass fiber cement core respectively.

4. DISCUSSION

The steel cement is the best design with regard to porosity. It has 7% less porosity compared to the neat cement. Cores from the silica sand and calcined clay designs have 1% and 3% less porosity respectively with reference to the neat cement. Due to the compactness of the porosity values, it can be said that the effect of the additives on the porosity is insignificant.

The permeability of the glass fiber design was approximately a magnitude of 10nD less than the rest of the cement designs. This is very critical in preventing corrosive acidic reservoir brine from penetrating into the cement and leaching out Ca out of the cement matrix. The variation in the porosity and permeability values for each design is related to the different microstructure present in the cement sheaths.

The SEM micrographs also provide information with regards to the chemical reaction between the silica (quartz) in the cement and the rest of the cement matrix. The quartz in most of the samples serves as foundation for the growth of C-S-H (Figure 1C). The only possible source for the Cl elements present in the pores of the samples and internal pores of the C-S-H is the curing brine which contains Na^+ and Cl^- as the hydration products of cement samples did not have these elements. A possible hypothesis for the presence of Cl in the cement matrix is that Cl^- from the brine was diffused into the cement pore water since the concentration of Cl^- was higher in the brine, and almost nonexistent in the cement pore water.

There is exchange of ions between the highly alkaline cement pore water and the brine when cement is in contact with brine. The brine is acidified by atmospheric CO_2, therefore it contains HCO^{3-} and CO_3^{2-} ions along with Na^+, K^+, Mg^{2+}, and Cl^- from the salt dissolved in the brine. Although the cement pore water is Na^+, K^+, and Mg^{2+} rich; their concentrations are much higher compared to those in the brine. This causes an inequilibrium leading to diffusion of those ions from the cement pore water into the brine. The outward diffusion of ions into the brine consequently reduces the pH of the cement pore water and initiate dissolution of $Ca(OH)_2$ from the cement sheath. As $Ca(OH)_2$ dissolves into the brine, the pH of the brine increases. The increase in the pH of the brines where cements were cured indicates that there is leaching of cement during the experiment. The cement cores are the only possible source for the higher Ca^{2+} that was observed in the cement brines since the control brine only showed traces of Ca^{2+}. This support the theory that $Ca(OH)_2$ is been dissolved from the cement matrix when in contact with low pH fluids.

The impact of the additives on the cement can be best observed in the compressive strength result and the TGA results. The consistent higher strength measured in the steel fiber design cores indicates they can be used to improve the strength of the cement in the proposed wellbore conditions. The difference between the amount of $Ca(OH)_2$ present on the outside and the inside of the cores in the TGA is critical when considering a wellbore. The outside of the core is very similar to the cement-formation interface where the cement is always in contact with the reservoir brine. The TGA result suggests there would be rapid dissolution of calcium from cement sheath at the cement–formation interface which would result in the formation of micro annulus along the cement-formation interface further exposing the cement sheath to degradation and also sustained casing pressure [23].

As predicted, the neat cement design had the highest amount of $Ca(OH)_2$ present in the original cement sheath as it does not have the advantage of the silica flour and other admixtures. For example, in the cement designs with silica flour there should be more calcium silicate hydrate and less $Ca(OH)_2$ in the cement cores compared to the neat cement due to the pozzolanic reaction between additivies and cement. Calcium hydroxide in the cement will combine with the silica flour to form calcium silicate hydrate which reduces permeability significantly and is more resistant to low pH geofluids than Portlandite (calcium hydroxide).

$SiO_2(am) + Ca(OH)_2(s) \rightarrow 3CaO{\cdot}2SiO_2{\cdot}3H_2O(s)$; formation of C-S-H from silica flour and $Ca(OH)_2$

5. CONCLUSION

The liquid pressure-pulse decay permeameter provides an accurate, time efficient way to measure cement permeability with the porosity known. Long, uneven fibers such as glass fibers can be used to reduce permeability in wellbore cement sheath.

For proposed wellbore (Feng et al., 2011), addition of steel fibers and glass fiber along with silica flour would be necessary to increase the durability cement sheath over life of the well under geopressured geothermal conditions. Further investigations are being carried out to evaluate cement/casing interfaces under such conditions.

TGA OF NEAT CEMENT CORE

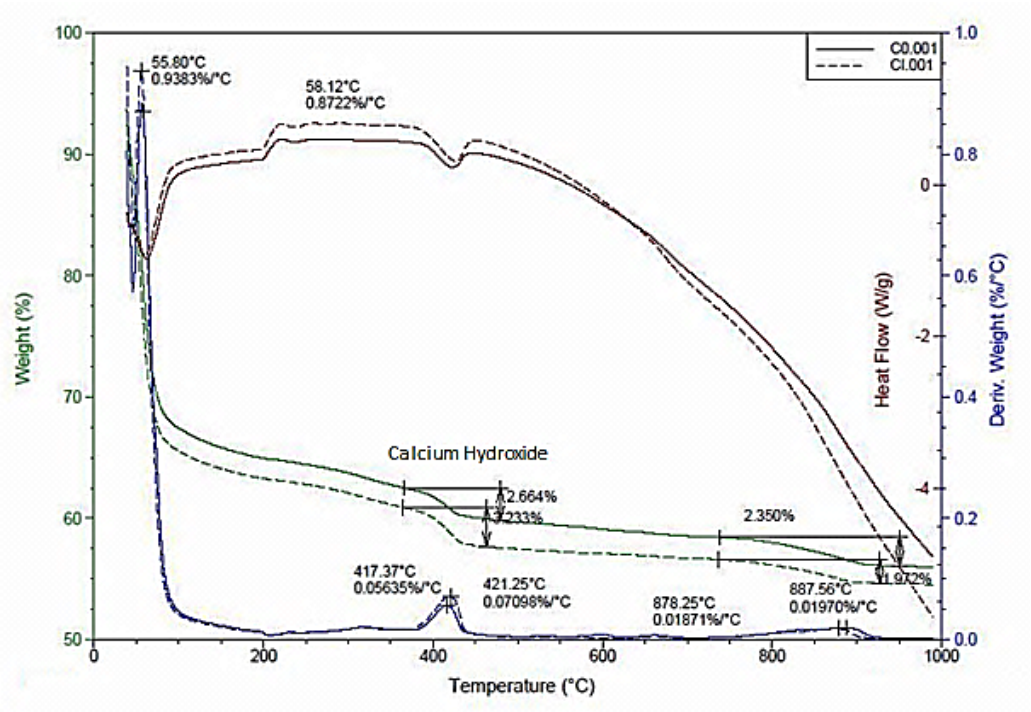

Figure 3: Plot of TGA comparison of the outside and inside of a neat cement core after 100 thermal cycles. Hashed lines were used to represent from inside the cement core while bold lines were used for the outside

TGA OF STEEL CEMENT CORE

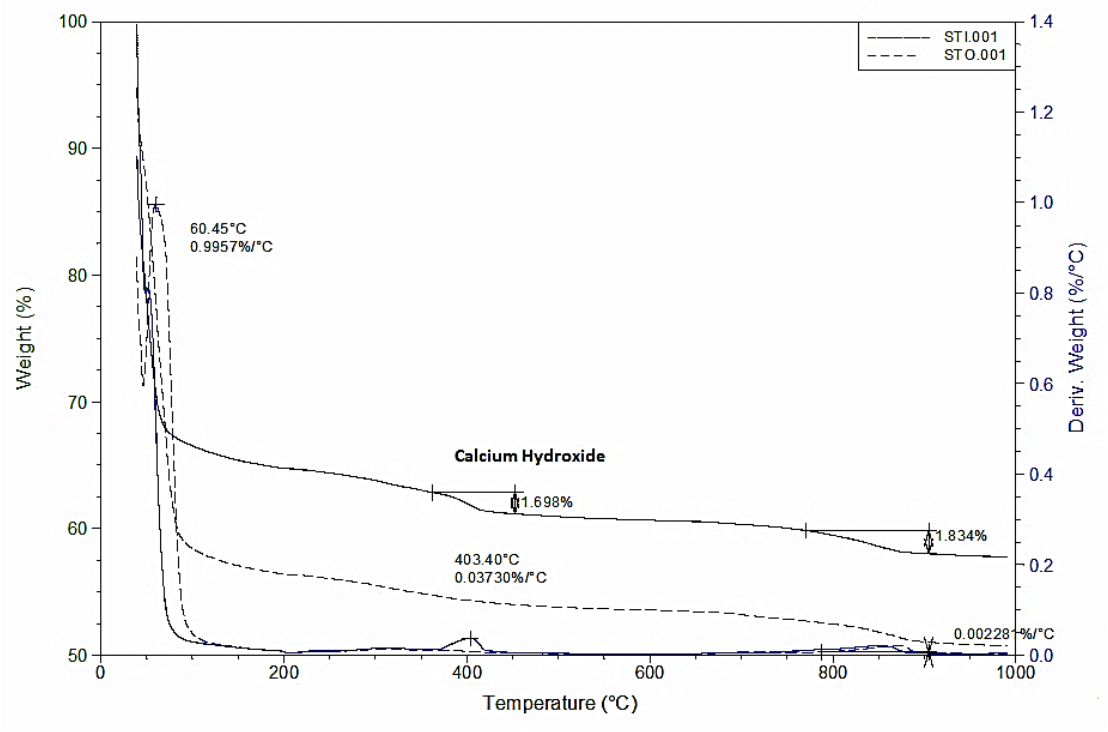

Figure 4: TGA plot showing comparison in steel cement after 100 thermal cycles. Hashed lines represent result from outside the cement core while bold lines were used for the inside of the core.

TGA OF SILICA SAND CORE

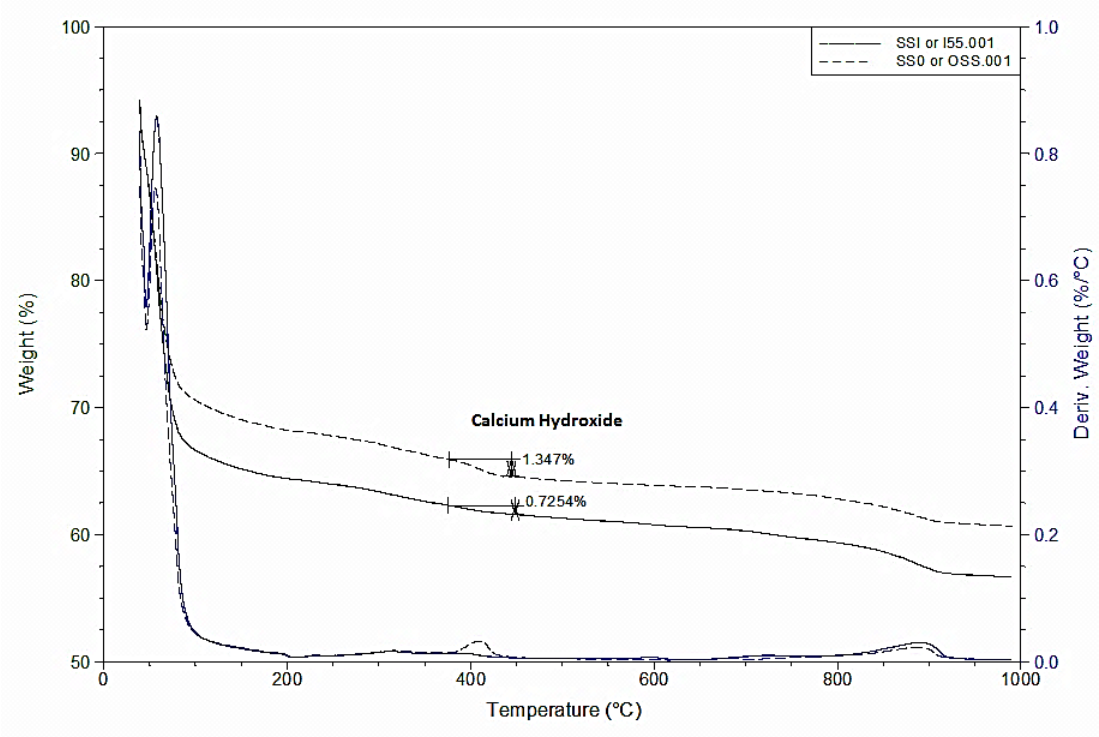

Figure 5: TGA plot comparing chemical changes on the surface of silica sand cement core to the inside of the core after 100 thermal loading cycles. Hashed lines represent result from outside the cement core while bold lines were used for the inside of the core.

TGA OF CALCINED CLAY CORE

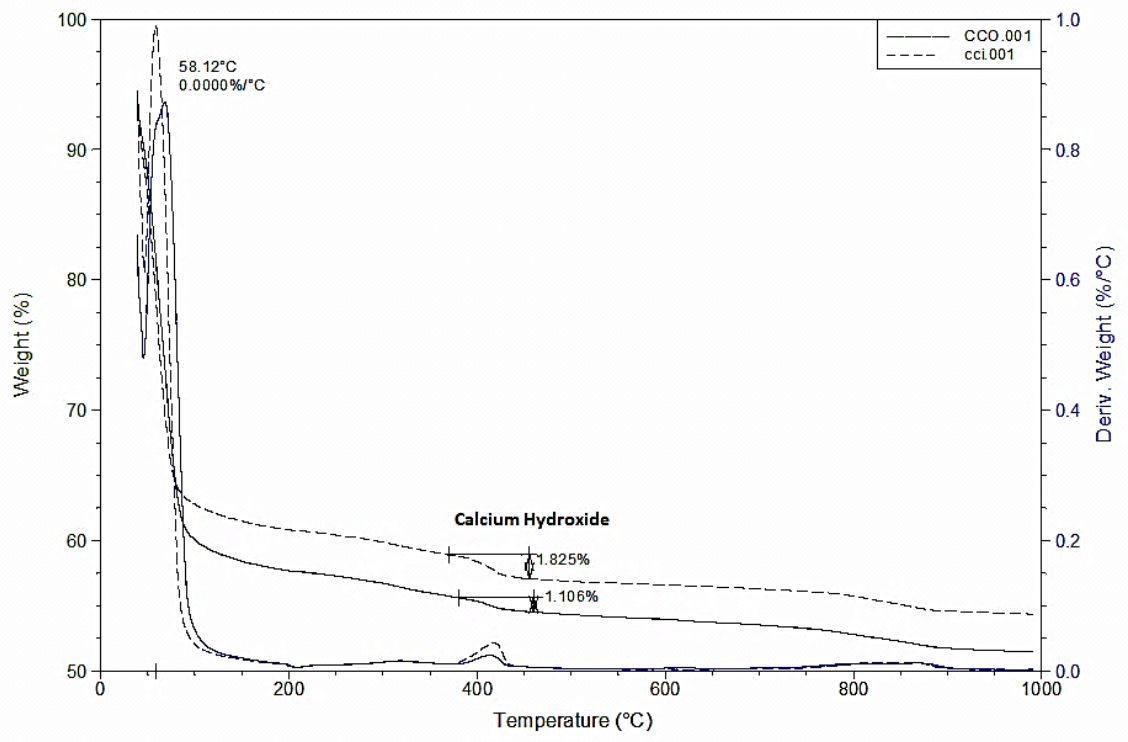

Figure 6: TGA plot comparing chemical changes on the surface of calcined clay cement core to the inside of the core after 100 thermal loading cycles. Hashed lines represent result from inside the cement core while bold lines were used for the sample from the surface of the core.

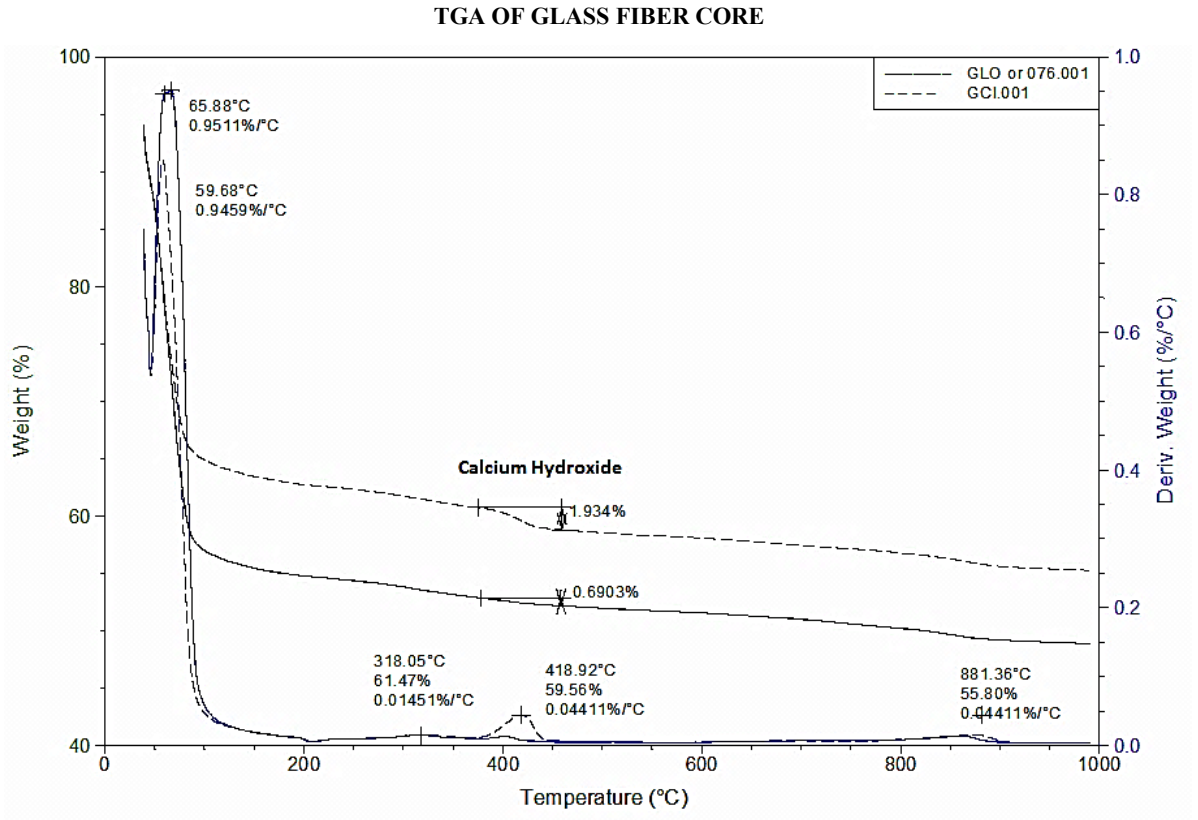

Figure 7: TGA plot showing comparison in glass cement after 100 thermal cycles. Hashed lines represent result from inside the cement core while bold lines were used for the sample from the surface of the core.

AKNOWLEDGEMENT

The authors wish to thank the Department of Energy for funding this project. We would also like to express our sincere gratitude to Richard DuBois of Halliburton Drilling Fluids Lab in Broussard, LA for his help with compressive strength measurements and providing us with silica flour, silica sand, steel fiber, and glass fibers. Lastly, we wish to thank Rodney Macon of TXI in Houston, TX for providing us with calcined clay.

REFERENCES

American Petroleum Institute (1977) Recommended practice for testing oil-well cements and cement additives. API Recommended Practice 10.12 ed. API 10B

Agbasimalo N, and Radonjic M (2014) Experimental study of the impact of drilling fluid contamination on the integrity of cement-formation interface. Journal of Energy Resources Technology (JERT), Vol. 136, No. 3.

Boulin PF, Bretonnier P, Gland N, Lombard JM (2012) Contributions of the steady state method to water permeability measurement in very low permeability porous media. Oil and Gas Science and Technologies-Rev. IFP Energies nouvelles. 67:387-401.

Chen T, and Stagg PW (1984) Semilog analysis of the pulse-decay technique of permeability measurement. Society of Petroleum Engineers. Doi: 10.2118/11818-PA.

Dorfman M (1982) The outlook for geopressured/geothermal energy and associated natural gas. In Journal of Petroleum Technology. 34, 9:1915-1919.

Dusseault M, Gray M, and Nawrocki P (2000) Why oilwells leak: cement behavior and long-term consequences. In *International Oil and Gas Conference and Exhibition in China*.

Feng Y, Tyagi M., and White CD (2011) Effect of natural convection patterns on optimal location and size of a heat sink in a geothermal reservoir. In proceedings of the 36th Workshop on Geothermal Engineering, Stanford University, Stanford, California.

Griggs J (2004) A re-evaluation of geopressured-geothermal aquifers as an energy resource. Master's Thesis. Louisiana State University.

Hanor JS, and Mercer JA (2010) Spatial variations in the salinity of pore waters in northern deep water Gulf of Mexico sediments: implications for pathways and mechanisms of solute transport. In Geofluids. 10:83-93

Herrin E (1975) Environmental problems associated with the production of energy from geopressured reservoirs, In proceeding of Geopressured Geothermal Energy Conference, Austin, Texas, 2 - 4 June, 1975.

Jones SC (1997) A technique for faster pulse-decay permeability measurements in tight rocks. SPE Formation Evaluation.

McCoy RL, Hartsock JH, Dobson RJ (1980) Preliminary results of the wells-of-opportunity geopressured-geothermal testing program. Presented at the SPE/DOE Symposium on Unconventional Gas Recovery, Pittsburgh, Pennsylvania, May 18 - 21, 1980

Oyibo A, and Radonjic M (2014) Inpact of Mud contamination on cement formation shear bond strength. OMAE San Francisco, CA

Scherer GW, Valenza JJ, Simmons G (2006) New methods to measure liquid permeability in porous materials. In Cement and Concrete Research. 37:386-397.

Sugama T (2006) Advanced cements for geothermal wells. Final report prepared for The U.S Department of Energies Office of Geothermal Technologies. Upton, New York: Brookhaven National Laboratory

Taylor HFW (1997) Cement Chemistry. Thomas Telford Services, London.

Yalkinkaya T, Radonjic M, Willson CS, and Bachu S (2011) Experimental study on a single cement-fracture using CO_2 rich brine. In Energy Procedia. 4:5335-5342